Functionalization of Carbon Nanotubes with Nickel Cyclam for the Electrochemical Reduction of CO 2

Silvia Pugliese, Ngoc Tran Huan, Jeremy Forte, Domenico Grammatico, Sandrine Zanna, Bao-Lian Su, Yun Li, Marc Fontecave

To cite this version:

Silvia Pugliese, Ngoc Tran Huan, Jeremy Forte, Domenico Grammatico, Sandrine Zanna, et al.. Functionalization of Carbon Nanotubes with Nickel Cyclam for the Electrochemical Reduction of CO 2. ChemSusChem, 2020, 10.1002/cssc.202002092 . hal-03034395

HAL Id: hal-03034395
https://hal.sorbonne-universite.fr/hal-03034395v1

Submitted on 1 Dec 2020

Functionalization of Carbon Nanotubes with Nickel Cyclam for the Electrochemical Reduction of CO_2

Silvia Pugliese,[1,2] Dr. Ngoc Tran Huan,[1] Jérémy Forte,[3] Domenico Grammatico,[2,4] Dr. Sandrine Zanna[5], Prof. Bao-Lian Su,[2] Yun Li,[1] Prof. Marc Fontecave[1]**

1. Laboratoire de Chimie des Processus Biologiques, UMR CNRS 8229, Collège de France-CNRS-Sorbonne Université, PSL Research University,11 Place Marcelin Berthelot, 75231 Paris Cedex 05, France.

2. Laboratory of Inorganic Materials Chemistry (CMI), University of Namur, 61 rue de Bruxelles, B-5000 Namur, Belgium

3. Sorbonne Université, Institut Parisien de Chimie Moléculaire, UMR 8232 CNRS, 4 place Jussieu, 75252 Paris Cedex 5, France

4. Bio-inspired Materials Group: Functionality & Self-assembly, Université de Pau et des Pays de l'Adour, E2S UPPA, CNRS, IPREM UMR 5254, 64000, PAU, France

5. Chimie ParisTech-PSL Research University-CNRS, Institut de Recherche de Chimie Paris (IRCP), 11 rue Pierre et Marie Curie, 75005 Paris, France

* to whom correspondence should be addressed : yun.xu-li@college-de-france.fr; marc.fontecave@college-de-france.fr

KEYWORDS: CO_2 electroreduction; nickel cyclam; pyrene; heterogenization; carbon nanotubes

Abstract

The exploitation of molecular catalysts for CO_2 electrolysis requires their immobilization on the cathode of the electrolyzer. As an illustration of this approach, a Ni-cyclam complex, with a cyclam derivative functionalized with a pyrene moiety, was synthesized, shown to be a selective catalyst for CO_2 electroreduction to CO and immobilized on a carbon nanotube-coated gas diffusion electrode by using a non-covalent binding strategy. The as-prepared electrode is efficient, selective, robust for electrocatalytic reduction of CO_2 to CO. Very high turnover numbers (ca. 61460) and turnover frequencies (ca. 4.27 s^{-1}) were enabled by the novel electrode material in organic solvent-water mixtures saturated in CO_2. This material provides an interesting platform for further improvement.

Introduction

Catalysis for CO_2 electroreduction into energy-dense products, such as CO, formic acid, hydrocarbons and alcohols, has attracted extensive research attention during the last 10 years as this reaction represents one of the most promising strategies for both CO_2 utilization as a carbon source and storage of intermittent renewable energy in the form of stable chemical energy. Catalysts are needed to overcome important kinetic limitations related to the multi-electron and multi-proton transfers associated with the CO_2 reduction reaction (CO2RR). Current research focuses on both heterogeneous materials[1–3] and homogeneous organometallic complexes.[4, 5] The former are favored industrially due to more facile product separation and catalyst regeneration and recovery. However, molecular compounds afford the opportunity to more easily design and synthetically tune the coordination environment of the active metal center. Mechanistic studies are also facilitated in that case. To reconcile these two approaches, homogeneous catalysts can be immobilized on heterogeneous conductive supports to generate cathode materials for electrolyzers. Such heterogenized molecular systems thus combine the advantages of a solid material (easy recovery of products and catalysts, efficient electron transfer from the electrode support to the catalyst, high Turnover Numbers) with those of molecular complexes (synthetic control of the electronic properties and the coordination environment of the active sites), while suppressing deactivation processes (such as dimerization) and solubility issues associated with the latter. This class of hybrid catalysts for CO2RR has been recently described in different review articles.[6–8]

Among various methods, a widely used and straightforward technique for immobilizing molecular catalysts is based on hydrophobic and $\pi-\pi$ stacking interactions between a carbon-based support, generally graphite electrodes or multi-walled carbon nanotubes (MWCNTs), and the molecular catalyst, as recently reviewed.[6–8] MWCNTs have the advantages of stability, high electrical conductivity and high surface area. While there have been some successes regarding heterogeneous immobilization of CO2RR catalysts on carbon supports such as MWCNTs, these are few and limited mainly to polyaromatic macrocyclic ligands.[8] For example, immobilization of a CO2RR molecular catalyst is possible without any functionalization of the ligand when the ligand is highly conjugated as in the case of metal porphyrins and phtalocyanines.[9–11] In contrast, when the ligand, such as bipyridine or benzene-based pincer derivatives, has a limited electronic delocalized structure, an aromatic group, most often pyrene, has to be covalently added to the ligand: the pyrene group allows tight grafting of the molecular complex on carbon electrode surfaces via $\pi-\pi$ stacking interactions. Regarding such simple ligands functionalized with a pyrene group, the most representative reports concern bipyridine-pyrene derivatives used to immobilize a [Re(bpy)(CO)$_3$Cl] complex on a graphite support[12] or a [Mn(bpy)(CO)$_3$Br] complex on carbon nanotubes[13] as well as a pincer-pyrene ligand used to immobilize an Iridium complex onto a gas diffusion electrode via carbon nanotubes.[14] The three materials displayed interesting electrochemical CO2RR catalytic properties, however in some cases with limited activity and stability.

In order to explore other classes of ligands, in particular non-aromatic in nature, and complexes based on non-noble metals, we have investigated one of the most studied molecular catalysts for CO2RR, namely [Ni(cyclam)]$^{2+}$ with cyclam = 1,4,8,11-tetraazacyclotetradecane. To our knowledge, while the heterogenization of [Ni(cyclam)]$^{2+}$ complex has already been proposed,[15, 16] there is no precedent for its non-covalent immobilization on a carbon-based nanostructured electrode. For that purpose, we have synthesized an original pyrene-cyclam derivative and the corresponding Ni complex, complex **1** in Scheme 1, which was found to be a unique 6-coordinated Ni cyclam complex. We report here the electrocatalytic properties of complex **1** both in solution and after immobilization on MWCNTS. The complex proved to behave as a very selective homogeneous catalyst for CO_2 electroreduction to CO in organic solvents in the presence of water. Furthermore, the presence of a pyrene moiety on the ligand was exploited to readily heterogenize the complex on MWCNTs via non-covalent interactions. The novel hybrid solid electrode, obtained by deposition of the functionalized MWCNTs on a Gas Diffusion Layer, was found to be active, stable and highly selective for CO_2 electroreduction to CO in acetonitrile-water solvent. These results illustrate the potential of immobilized molecular catalysts for CO_2 electroreduction, a class of materials yet to be developed for such an application.

Results

Complex synthesis and characterization

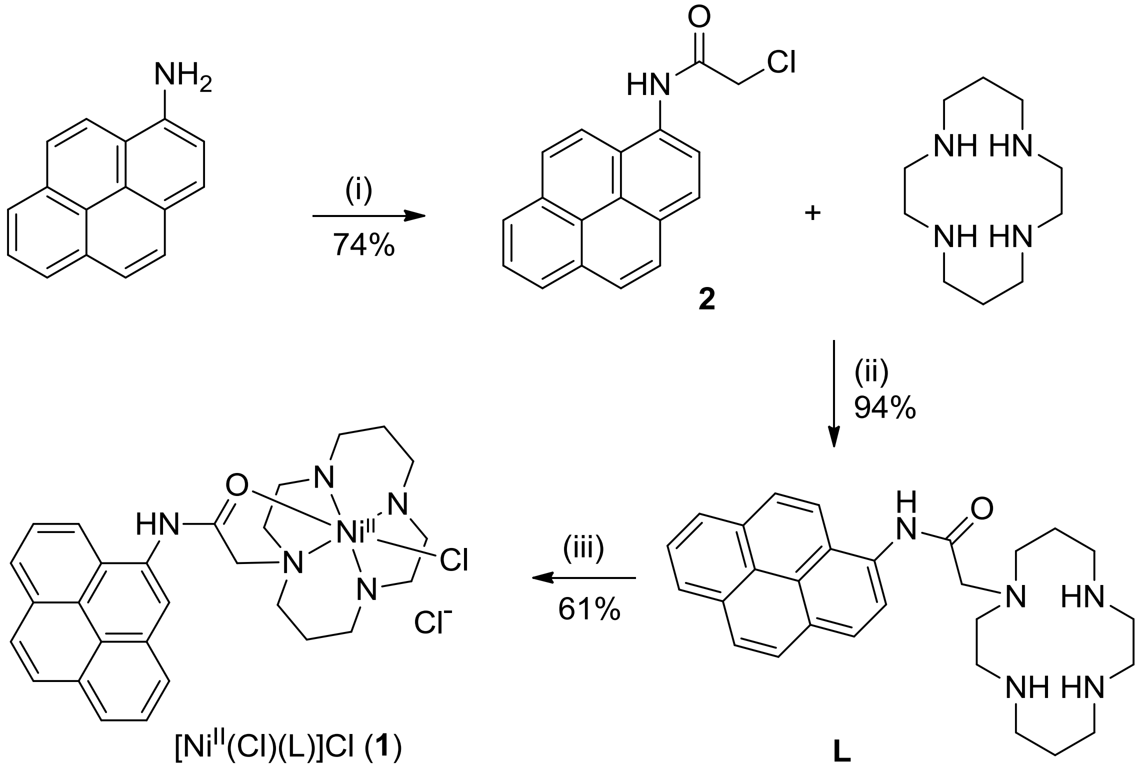

Scheme 1. Synthesis of complex **1**. Conditions: (i) $ClCH_2COCl$, NEt_3, CH_2Cl_2; (ii) K_2CO_3, KI (cat.), CH_3CN; (iii) $NiCl_2.6H_2O$, EtOH.

In order to synthesize a $[Ni(cyclam]^{2+}$ complex bearing a pyrene group, we chose to prepare the ligand **L**, in which one N atom of the cyclam ring is alkylated with a substituent containing a pyrene moiety (Scheme 1), according to a previously reported procedure.[17] However, this previous synthesis gave the product in low yields and required arduous chromatographic purification. In this work, we improved the experimental procedure, especially for the N-alkylation of the cyclam ring step, by replacing the chromatographic purification step with washing with water, and **L** could be easily synthesized on a large scale. The corresponding nickel complex $[Ni^{II}(Cl)(L)](Cl)$ (**1**) was obtained using nickel chloride hexahydrate in ethanol for metallation.

Complex **1** was isolated in the form of crystals suitable for X-ray analysis. Crystal data of all obtained structures are available in Table S1. Four different solvents, ethanol (EtOH), acetonitrile (CH_3CN), dichloromethane (CH_2Cl_2) and N,N-dimethylformamide (DMF) were used for crystallization, resulting in different crystal packings differentially stabilized by intermolecular hydrogen bonding, π-stacking and Van der Waals interactions (Table S1). In all structures, the nickel center ion was found in a distorted octahedral coordination geometry, with a chloride ion and the oxygen atom of the amide carbonyl group occupying two ligand positions and completing the four coordinating nitrogen atoms of the cyclam ring. However, two different structures, with different configurations, were obtained, reflecting the presence of two isomers, named *trans*-**1** and *cis*-**1** in the following. Four crystal structures of *trans*-**1** and two crystal structures of *cis*-**1** were solved (Tables S1 and S2). In *trans*-**1**, which crystallized in all solvents used, Cl and O ligands occupy the axial positions and are thus *trans* to each other with respect to the Ni ion, while the four positions of the equatorial plane are occupied by the N atoms of the cyclam ring (Figure 1a). For the *cis*-**1** isomer, which crystallized in EtOH and DMF, Cl and O ligands are *cis* to each other: the equatorial plane is constituted by three N atoms of the cyclam ring (two secondary and one tertiary amines) and a Cl ligand while the apical positions are occupied by the O atom of the amide carbonyl group and the fourth N atom (one secondary amine) of the cyclam ring (Figure 1b). In the two isomers, the nickel ion, the tertiary nitrogen atom and the carbonyl oxygen atom are together part of a five-membered ring with two carbons from the dangling substituent (Figure 1). Each isomer is a racemic mixture of two enantiomers (only the *R,S,S,R* *trans*-**1** and the *S,S,S,S* cis-**1** are shown in Figure 1).

Bond lengths and angles values for all obtained crystal structures are given in Table S2. The Ni-O bond lengths are in the range of those of Ni-N (between 2.05 and 2.14 Å), while the Ni-Cl bond lengths (between 2.40 and 2.45 Å) are slightly longer. All these values are close to those of a similar octahedral [Ni(cyclam)(OH_2)(Cl)]Cl complex, previously reported by Zhanaidarova and al (Ni-O distance : 2.17 Å and Ni-Cl distance : 2.52 Å).[16]

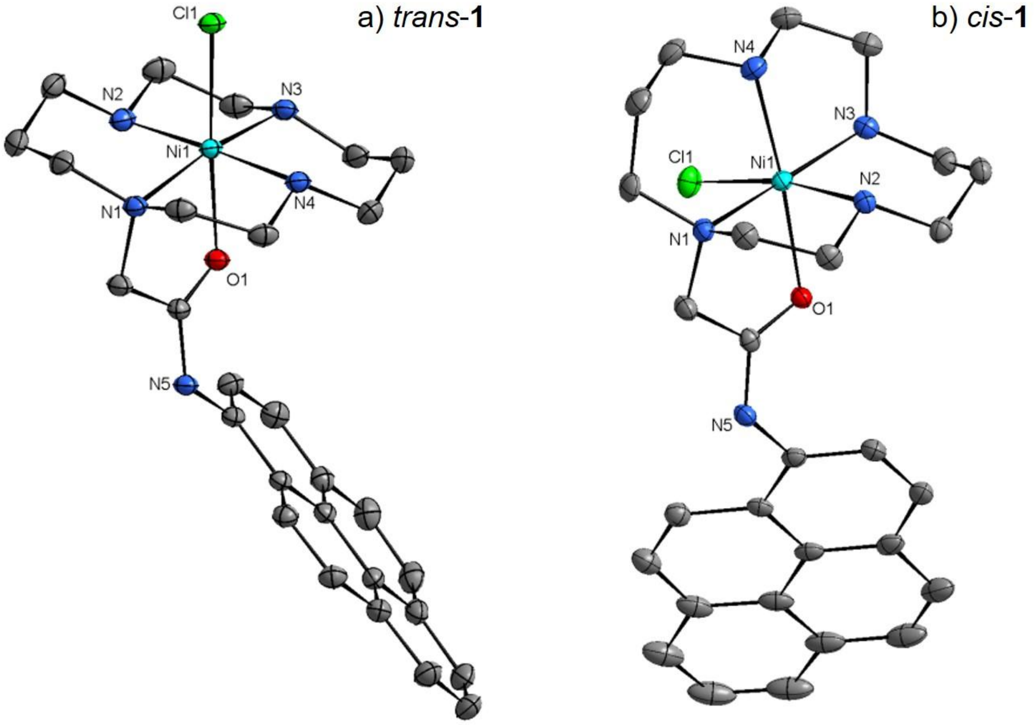
a) *trans*-**1**

b) *cis*-**1**

Figure 1. Crystal structure representation of the cation part of complex **1**. Ellipsoids are drawn with 30% probability. All hydrogen atoms are omitted for the sake of clarity. (a) *R,S,S,R trans*-**1** (from crystallization in CH_3CN); (b) *S,S,S,S cis*-**1** (from crystallization in DMF). Only one of the enantiomers is shown in both cases.

The electrochemical properties of complex **1** were studied in DMF, with all potentials vs. Fc^+/Fc^0. Figure 2 (dotted, dashed and black) shows the complex cyclic voltammograms (CVs) of complex **1** (1 mM) in DMF with 0.1 M $TBAPF_6$ as a supporting electrolyte on a glassy carbon disk (3 mm diameter) as a working electrode, under an argon atmosphere, when scanned down to either -2.38, -2.62 or -3.1V. The complexity comes from the fact that two different complexes, *trans*-**1** and *cis*-**1**, are present in solution and that the ligand itself is redox-active due to the presence of pyrene.[18] The first feature at -2.28 V was assigned to the one-electron reduction of Ni^{II} to Ni^{I}, approximately 180 mV more cathodic than for the unfunctionalized $[Ni(cyclam)]^{2+}$ complex peaking at -2.1 V (Figure 2, red), in agreement with a much more electron-enriched Ni center in complex **1** due to the presence of extra electron-donating ligands. As a confirmation of this assignment to the metal site, this feature was absent on the CV of the unmetallated pyren-cyclam ligand, **L** (Figure 2, blue). This signal is irreversible in all CVs even when reversing the scan immediately after the reduction peak, in contrast to that of $[Ni(cyclam)]^{2+}$ (Figure 2). This indicates de-coordination of Cl or/and O ligands upon reduction. Quite often, a small shoulder was present at -2.1 V, likely corresponding to a very small amount of the complex without Cl/O coordination, likely in equilibrium with complex **1** in solution. A second complex irreversible feature appeared at slightly more cathodic potential (from -2.38 to -2.65 V) and proved difficult to assign. It could possibly have contributions in part from the one-electron reduction of the pyrene ring, even though the pyren-cyclam ligand, **L**, exhibits a reversible signal in this potential region (Figure 2, blue). Finally, upon scanning down to below -3.0 V, a signal at -2.86 V was observed and assigned to Ni^{I} to Ni^{0} reduction. This signal is indeed absent within the CV of the unmetallated pyrene-cyclam ligand and is also present in the CV of $[Ni(cyclam)]^{2+}$ upon scanning at a potential (- 2.55 V) allowing Ni^{I} to Ni^{0} conversion (Figure S1). On the oxidizing return scan, the feature at + 0.2 V, also found in the unmetallated pyrene-cyclam ligand, is assigned to ligand oxidation (Figure 2). The broad signal at -0.66 V was exclusively seen after scanning down to a very negative potential, and not when the cathodic scan was reversed after the second reduction wave at – 2.62 V. This is consistent with Ni^{0} species generated at negative potentials and adsorbing on the surface of the electrode where they get oxidized to Ni^{II} at -0.66 V during the back scan. A similar situation was observed with the unfunctionalized $[Ni(cyclam)]^{2+}$ complex when scanning down to very negative potentials (Figure S1).

The cathodic peak current density (j_p) at -2.28 V varied linearly with the square root of the scan rate ($v^{1/2}$) from 0.01 to 0.5 Vs^{-1} under Ar, consistent with diffusion-controlled processes and thus with active complex **1** remaining in solution (Figure S2). We also verified that no adsorption of the complex occurred at the surface of the GC electrode. Indeed, when, after 30 cycles of CV, the electrode was removed from the electrolyte and used in a fresh electrolyte without complex **1**, no signal corresponding to complex **1** could be observed in the CV.

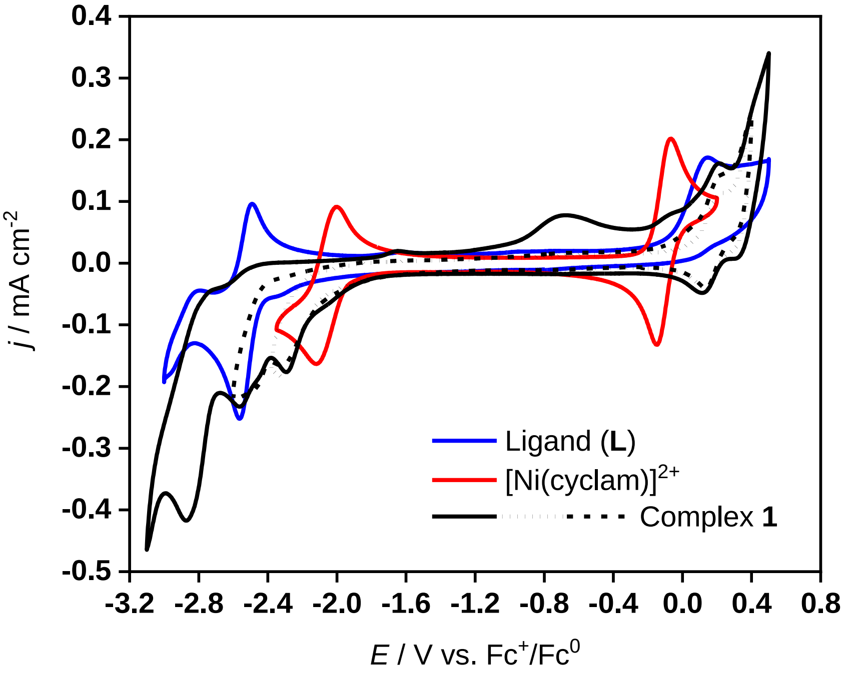

Figure 2 Cyclic voltammograms of complex **1** (black, dashed and dotted), $[Ni(cyclam)]^{2+}$ (red), ligand (**L**, blue). Conditions: DMF with 0.1M $TBAPF_6$ as the electrolyte, under Ar and at room temperature. Concentrations were 1 mM for all species. Scan rate 100 mV s^{-1}.

*CO_2 reduction catalyzed by complex **1***

Upon addition of CO_2, in the absence of a source of protons, the CV of 1 mM complex **1** (Figure S3) presented a small catalytic wave with an increase of current density and a potential at half-peak catalytic current of about -2.16 V, more anodic that of the Ni^{II} / Ni^{I} signal and with an onset potential close to that of [Ni(cyclam)]$^{2+}$. In line with previous reports on CO_2 electroreduction catalyzed by [Ni(cyclam)]$^{2+}$, this wave is assigned to the catalytic reduction of CO_2 to CO during which reduction of Ni^{II} to Ni^{I} promotes de-coordination of Cl/O ligands and allows Ni^{I} to bind and activate CO_2 within a liberated coordination site.[19]

However, given the importance of protons in the CO2RR in general and specifically for CO2RR catalyzed by [Ni(cyclam)]$^{2+}$,[20] the effect of increased concentrations of H_2O was studied by CV and bulk electrolysis. As expected, the catalytic current increased further upon addition of H_2O, from 0.4 M to 2 M (Figure S4a). Considering a CO/CO_2 reduction potential in a DMF–water solvent mixture at - 1.41 V vs. Fc$^+$/Fc^0 (CO/CO_2 potential is reported to be - 0.690 V vs. NHE[21] and the Fc$^+$/Fc^0 potential is reported to be 0.720 V vs. NHE in DMF,[22] the observed onset potential at -1.95 V corresponds to an overpotential of about 540 mV. In the absence of CO_2, a catalytic current, assigned to proton reduction to hydrogen, also increased upon increasing the concentration of H_2O (Figure S4b), however with an onset potential more cathodic than that for CO_2 reduction. This reflects the greater potential of complex **1** to catalyze the reduction of CO_2. Catalysis was similarly stimulated when using 2,2,2-Trifluoroethanol (TFE) as a proton source (Figure S5). In the following, only H_2O was considered as the proton source.

A controlled-potential electrolysis (CPE) was then carried out at -2.39 V during which reaction products were analyzed and quantified, either by gas chromatography (for CO and H_2), by Ionic Exchange Chromatography (for HCOOH) and ^{1}H NMR (for CH_3OH). For that purpose, the electrochemical cell used a 1 cm^2 GC plate as the working electrode and the electrolyte was a solution of complex **1** (1 mM) in CO_2-saturated DMF containing 0.1 M TBAPF$_6$ and 2 M H_2O as a proton source. CVs obtained with such a cell reproduced nicely the above CVs (Figure S6a). After 60 minutes electrolysis (Figure S6b), CO was found as the only reaction product in the gaseous phase (faradaic yield: 96%) and no formate could be detected in the liquid phase. The catalyst proved quite robust during 1 hour electrolysis as shown from the stability of the current density, while its activity is limited as shown by the low current density (0.3 mA.cm^{-2}). As a further proof of the stability of the catalyst, a CV recorded after CPE was found to be comparable to that before electrolysis, except for a small decrease in intensity (Figure S6a). The same experiment but in the absence of complex **1** did not yield any CO_2 reduction products.

*Immobilization of complex **1**: preparation of the hybrid electrode and characterization*

Complex **1** was immobilized on MWCNTs through the establishment of π-π stacking interactions between the pyrene moieties and graphene motifs. In the first step, MWCNTs (2 mg) were first sonicated in ethanol in the presence of Nafion, then drop-casted on a 1 cm^2 surface of commercial gas diffusion layer (GDL), consisting of a carbon fibres cloth coated with a micro-porous Teflon layer embedding carbon black so as to keep electronic conductivity properties. Then the MWCNT/GDL electrode was dipped into a solution of 10 mM complex **1** in DMF, left overnight and then washed with water and acetonitrile to remove any loosely bound complexes, and finally air-dried before electrochemical experiments.

The **1**/MWCNT/GDL electrode was characterized by Scanning Electronic Microscopy (SEM) and X-ray photoelectron spectroscopy (XPS). As shown in Figure S7a, a porous network of MWCNTs was observed in SEM images after functionalization. XPS analysis (survey spectrum) confirms the presence of Ni and N atoms, from complex **1**, on the surface of the electrode, together with O atoms from alcohol or carboxylic acid defects of pristine MWCNTs (Figure S8 and Table S3). A Ni $2p_{3/2}$ signal is observed at 855.9 eV in good agreement with the presence of a Ni^{II} ion. Since there is fluoride in the deposited materials coming from Nafion with the F auger peak masking the Ni 2p signal at 861.47 eV, a control MWCNT/GDL electrode in the absence of complex **1** has been also analysed by XPS. The peak decomposition allowed to identify the signal of Ni 2p (Figure S8 and Table S1) and the ratio of N/Ni is 4.5 approximately, whereas the N 1s peak was centered at 400.4 eV.

The **1**/MWCNT/GDL electrode was also characterized by Cyclic Voltammetry. CVs were recorded in CH_3CN containing 0.1M $TBAPF_6$, using such **1**/MWCNT/GDL electrode (Figure S9). The high capacitive currents observed in the voltammograms are explained by the 3D structure and the high surface area of the working electrodes. Integration of the signal at – 1.7 V vs. Fc^+/Fc^0 corresponding to Ni reoxidation from Ni^I to Ni^{II} allowed to determine a concentration of electroactive species for the complex of 5 10^{-9} mol cm^{-2} (see experimental section). Such a value is in line with previously reported values for MWCNTs functionalized with molecular Ni complexes.[23] The intensity of that peak was directly proportional to the scan rate, thus confirming the immobilization of the nickel complex onto the electrode surface (Figure S9).

*Immobilization of complex **1**: electroreduction of CO_2.*

The electrochemical reduction of CO_2 using the new electrode material was carried out in CH_3CN containing 0.1M $TBAPF_6$ as the electrolyte, in the presence of 1% H_2O as a proton source, after saturation with CO_2. A linear sweep voltammogram (LSV) shows a catalytic wave occurring at more anodic potentials as compared to the MWCNT/GDL control electrode (Figure 3a).

Chronoamperometric measurements were carried out at various potentials from – 2.34 to – 2.74 V vs. Fc^+/Fc^0 for 20 min (Figure 3b). The current density proved stable in all cases. As a matter of fact, the same electrode could be used for several independent electrolysis experiments without any loss of activity. The CO_2 reduction products distribution, in terms of faradaic yields (FY), is shown in Figure 3c. CO was the major product at all potentials, with the highest FY value (92%) obtained at – 2.54 V vs. Fc^+/Fc^0 (with a current density of 6 $mA.cm^{-2}$). In all cases H_2 accounted for less than 11% and no formate could be detected. As a control experiment, CPE using a MWCNT/GDL electrode was performed at – 2.54 V vs. Fc^+/Fc^0 during 20 min (Figure S10a). Not only the current density was much lower (2.3 $mA.cm^{-2}$) but the system was selective for H_2 production instead (FY= 83% with a FY for CO of 4%). As a further control experiment, a CPE of **1**/MWCNT/GDL at – 2.54 V vs. Fc^+/Fc^0 was also run under Ar (Figure S10b). Only H_2 was produced after 20 min with no detectable CO_2 reduction products. Finally, CPE experiments were carried out at - 2.54 V vs. Fc^+/Fc^0 for 20 min with increased amounts of water (3% and 5%). As expected, the system became much less selective for CO_2 reduction, leading to FY for CO of only 22% and 12%, respectively.

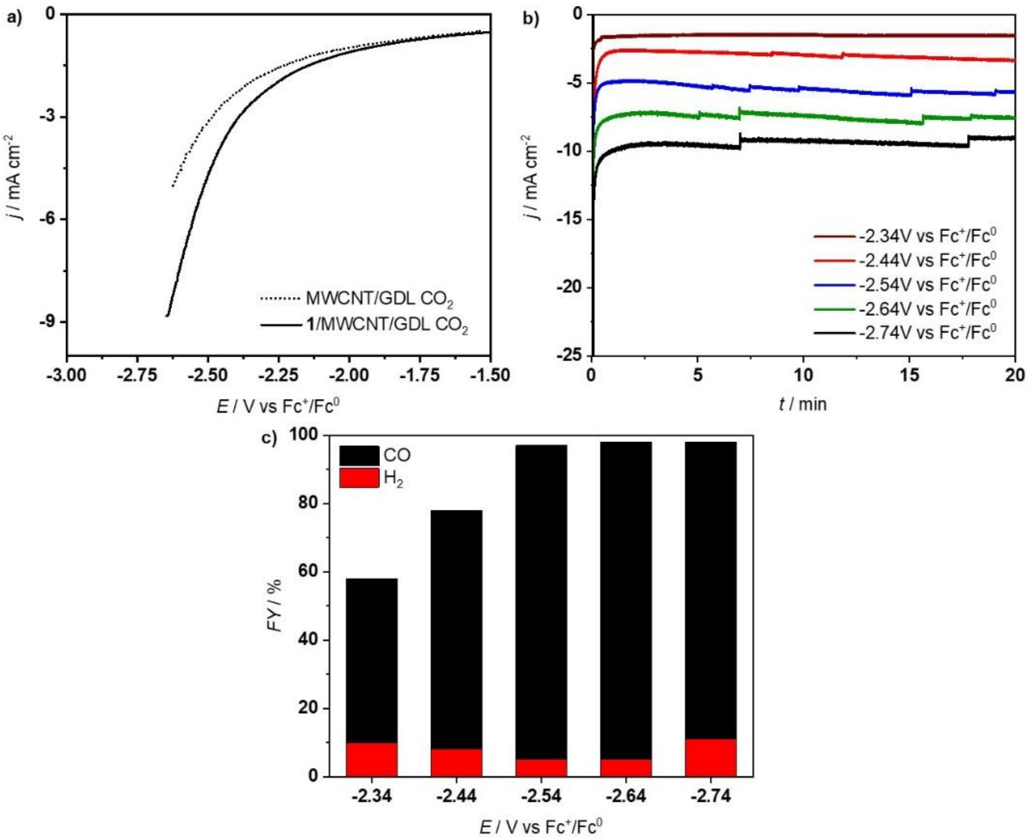

Figure 3. (a) LSV of **1**/MWCNT/GDL (black) and MWCNT/GDL (dotted) in acetonitrile with $TBAPF_6$ 0.1 M and H_2O 1% under CO_2. Scan rate 10 mV s^{-1}. (b) Controlled Potential Electrolysis using **1**/MWCNT/GDL as the electrode at different potentials under the same conditions. (c) Faradaic yields for CO and H_2 after 20 min electrolysis at different potentials.

A longer experiment (4h) carried out at - 2.54 V vs. Fc^+/Fc^0 using the **1**/MWCNT/GDL electrode under CO_2 confirmed the stability of the catalytic material as well of its selectivity with a FY for CO of more than 90% after 4h electrolysis (Figure S11). SEM (Figure S7b) as well as XPS (Figure S12) analysis after 4h electrolysis showed no substantial change in the structure of the electrode. In the XPS spectrum, the Ni 2p signal was identical to that before electrolysis (Figure S12c). The decomposition of N1s also confirmed the presence of cyclam (N 1s signal at 400.3 eV), while an additional signal was observed at around 403 eV, typical of quarternary ammonium such as TBA present in the electrolyte. The ratio of N/Ni was 4.05 approximately, close to the value before electrolysis.

Based on the amount of electroactive sites on the surface of the electrode (5 10^{-9} mol cm^{-2}), a remarkable Turnover Number for CO formation of 61460 was obtained after 4 h electrolysis, corresponding to a Turnover Frequency value of 4.27 s^{-1}.

Discussion

For the sake of immobilizing a $[Ni(cyclam)]^{2+}$ complex at the surface of an electrode, a novel cyclam derivative carrying a pyrene moiety has been readily synthesized. This class of complex has been chosen not only because $[Ni(cyclam)]^{2+}$ is known to be a good, stable and selective molecular catalyst for CO_2 electroreduction and it is based on a non-noble metal but also because, to our knowledge, there is only one precedent for carbon electrode surface modification with $[Ni(cyclam)]^{2+}$ [16]. A $[Ni(cyclam)]^{2+}$ complex modified with a carboxylic acid group was used to for grafting onto titanium(zirconium) oxide surfaces but the resulting material was only studied for its properties in photoelectron transfer.[15] The new complex **1** is a 6-coordinated Ni complex, in which the tetranuclear N-based coordination of the cyclam ring is completed by a chloride anion and the oxygen atom of the amide group of the dangling substituent, with two different configurations, *trans* and *cis*, with respect to the relative positions of the Cl and O ligands. Coordination to a Ni^{II} center by the oxygen atom of a pendant amide group has been recently reported in the case of substituted cyclen complexes of Ni^{II}.[24] Complex **1** is thus the first $[Ni(cyclam)]^{2+}$ complex carrying a pyrene substituent.

Characterization of the electrochemical properties of complex **1** in DMF/H_2O using a glassy carbon electrode has revealed the following features. First, upon one-electron reduction of Ni^{II} to Ni^{I}, the complex enjoys decoordination of the Cl/O ligand(s); this is very important since the Ni^{I} state is the active species for CO_2 binding and activation, a process that requires a free Ni coordination site. Second, catalysis for CO_2 electroreduction occurs at the Ni^{II} / Ni^{I} redox process, as shown by cyclic voltammetry, which indicates that the mechanism of the reaction catalyzed by complex **1** follows that of $[Ni(cyclam)]^{2+}$.[25] Third, as in the case of $[Ni(cyclam)]^{2+}$ CO_2 reduction catalyzed by complex **1** is very selective for CO production (FY = 96%). Fourth, as expected, the activity is quite weak, providing only small current densities; indeed, $[Ni(cyclam)]^{2+}$ has been shown to be poorly catalytically active when using a glassy carbon electrode, while the best activities were obtained using a mercury electrode, on which the complex adsorbs and enjoys an increased reactivity both in organic and aqueous electrolytes. [19, 20, 26]

The pyrene-modified complex **1** has been immobilized on carbon nanotube-coated gas diffusion electrode using a non-covalent approach and the novel electrode, **1**/MWCNT/GDL, has been characterized electrochemically for CO_2 electroreduction. Under such an heterogenized configuration, complex **1** retained its high selectivity for CO production (FY above 90%), with H_2 accounting for less than 15%. More interestingly, it was shown to be much more active in the immobilized form than under homogeneous conditions: current densities up to 10 $mA.cm^{-2}$ could be obtained as compared to 0.3 $mA.cm^{-2}$ for a 1 mM solution of complex **1**. Finally, the derivatized electrode proved highly stable leading to impressive turnover numbers (61460 after 4 h electrolysis). This is remarkable since the electrode support is carbon-based and not mercury, so far the best electrode material for CO_2 electroreduction catalysed by $[Ni(cyclam)]^{2+}$: this might indicate that the stable interaction between complex **1** and the carbon surface of the MWCNTs specifically favors the most reactive conformations of the complex and disfavors CO poisoning, CO desorption being the turnover-limiting step of the catalytic cycle, as does mercury for the soluble $[Ni(cyclam)]^{2+}$ complex.[20, 26] As a consequence, complex **1** is one of the very best molecular catalysts, after immobilization onto an electrode surface, reported so far for CO_2 electroreduction, as discussed below.

The only previous attempt to graft a $[Ni(cyclam)]^{2+}$ complex on a solid electrode (in that case a covalent grafting onto a glassy carbon electrode) was achieved by Kubiak and coworkers, using electrooxidation of a terminal alkyne attached to the cyclam ring.[16] This led to a cathode material which proved poorly active (with current densities below 1 $mA.cm^{-2}$) and poorly selective for CO_2 reduction to CO (FY_{CO} = 7%; FY_{H2} = 89 %) under potential and solvent conditions comparable to those used here. The present work thus represents a great improvement regarding the utilization of solid electrodes functionalized with [Ni(cyclam)]$^{2+}$. This is due in great part to the large surface area and the nanostructuration of the CNTs support which allow a greater density of electroactive species. As a matter of fact, the **1**/MWCNT/GDL electrode is also much more efficient for CO_2 reduction to CO than a glassy carbon electrode functionalized with a [Re(bpy)$(CO)_3$Cl] complex using the same pyrene-dependent approach: the latter could achieve only 58 TONs during 1 hour electrolysis, after which the activity was lost.[12] Finally, the **1**/MWCNT/GDL electrode compares well with and complements the carbon nanotube-coated gas diffusion electrode derivatized with a molecular iridium pincer dihydride catalyst, which allows high TONs (200000 in 8 hours) of formate with high selectivity (> 90%) from CO_2 electroreduction in aqueous electrolytes.[14] While based on a noble metal, the latter is a reference material with respect to carbon electrodes functionalized with a molecular catalyst for CO_2 reduction. Indeed, while [Mn(bpy)$(CO)_3$Br] was also attached to MWCNTs via π-π interactions of a pyrene group, present in a bpy ligand derivative, with the CNT sidewalls, the resulting material proved much less active (low current densities), less stable, less selective (giving a mixture of CO and HCOOH together with H_2 as the major product) and achieving TONs of about 1500 after 8 h electrolysis under aqueous conditions.[13]

In conclusion, the present study confirms the benefits of incorporation of molecular catalysts onto electrode surfaces using the pyrene-CNT approach for CO_2 electroreduction. More specifically, it shows that the [Ni(cyclam)]$^{2+}$ complex provides an excellent platform on which further improvements of hybrid electrodes can be brought.

Experimental Section

General

All starting materials were commercially available (Sigma and TCI) and were used without further purification. Solvents were purified by an MBRAUN SPS-800 Solvent Purification System. All reactions were carried out under air atmosphere unless specified. ^{1}H and NMR spectra were recorded on a Bruker Avance-III 300 NMR spectrometer (300 MHz) at room temperature. UV-Vis spectra were recorded using a Cary 100 UV-Vis spectrophotometer instrument (Agilent).

*Synthesis of Complex **1***

2-Chloro-*N*-pyren-1-yl-acetamide (2). The synthesis was carried on as previously described with slight modifications.[27] Under an Ar atmosphere, 1-aminopyrene (5.45 g, 25.1 mmol) and triethylamine (5.6 mL, 40.1 mmol) were dissolved in CH_2Cl_2 (500mL), and chloroacetyl chloride (2.8 mL, 35.1 mmol) was added dropwise via a syringe. After 12 h of stirring under Ar, the precipitate was filtered, washed with H_2O and cold CH_2Cl_2 several times. The crude product was dried under vacuum over night to yield the product as a pale-grey powder which was used for the next step without further purification (5.49 g, 74%). ^{1}H NMR ($CDCl_3$, 300 MHz) δ 9.01 (br s, 1H), 8.45 (d, J = 8.3 Hz, 1H), 8.21-8.14 (m, 4H), 8.07-7.99 (m, 4H), 4.42 (s, 2H). This spectrum is identical to the reported one.[27]

***N*-Pyren-1-yl-2-(1,4,8,11-tetraazacyclotetradec-1-yl)-acetamide (L)**. This ligand was synthesized according to a reported method with slight modifications.[17] Under an Ar atmosphere, a mixture of cyclam (3.25 g, 16.2 mmol), 2-chloro-*N*-pyren-1-yl-acetamide (**2**) (940 mg, 3.2 mmol), K_2CO_3 (2.24 g, 16.2 mmol) and KI (270 mg, 1.6 mmol) in CH_3CN (677 mL) was heated under reflux. After 24 h, the solvent was evaporated under reduced pressure and the residue was washed with water and ether several times. The crude product was dried under vacuum overnight to yield the product as an off-white powder which was used for the next step without further purification (1.46 g, 94%).^{1}H NMR ($CDCl_3$) δ 11.4 (br s, 1H), 8.27 (d, J = 9.3 Hz, 1H), 8.19-7.96 (m, 8H), 3.44 (s, 2H), 2.90 (t, J = 5.4 Hz, 2H), 2.80 (m, 8H), 2.42 (t, J = 5.1 Hz, 2H), 2.3 (t, J = 5.1 Hz, 2H), 2.12 (m, 2H), 1.95 (m, 2H), 1.49 (m, 2H). This spectrum is identical to the reported one. [17]

Complex [Ni^{II}(Cl)(L)]Cl (1). A solution of **L** (100 mg, 0.11 mmol) in EtOH (2 mL) was added dropwise to a solution of $NiCl_2.6H_2O$ (52 mg, 0.11 mmol) in EtOH (2 mL). The pale green solution turned immediately to orange then dark pink. After 3h at room temperature, the solvent was evaporated to dryness and the blue-pink solid was dissolved in EtOH (6 mL) and ether was allowed to slowly diffuse to this solution to give complex **1** as a pink-purple powder (78 mg, 61%). UV-Vis [DMF]: λ nm (ε, M^{-1} cm^{-1}): 543 (10.7), 389 (1880), 353 (10920), 343 (15000), 329 (10000), 277 (16300), 266 (11060).

Single crystals suitable for X-ray diffraction were obtained by slow diffusion of Et_2O into a solution of DMF containing **1** at room temperature. CH_3CN, EtOH and CH_2Cl_2 were also used instead of DMF giving suitable single crystals. CCDC 2021920 *(trans*-**1**, MeCN), 2021925 *(trans*-**1**, EtOH), 2021922 *(trans*-**1**, DMF), 2021923 *(trans*-**1**, DCM), 2021921 *(cis*-**1**, EtOH) and 2021924 *(cis*-**1**, DMF) contain the supplementary crystallographic data for this paper.

Homogeneous Electrochemical Studies

All electrochemical experiments were performed on a VSP300 potentiostat (Bio-Logic Science Instruments SAS) and were conducted at room temperature in *N*,*N*-Dimethylformamide (DMF). 0.1 M tetrabutylammonium hexafluorophosphate ($TBAPF_6$) was used as the supporting electrolyte. The cyclic voltammetry (CV) experiments were carried out in a three electrode setup, with a 3 mm diameter glassy carbon (GC) electrode as a working electrode, which was polished on a polishing cloth with a 1 μm diamond suspension (Struers), sonicated for 10 seconds, thoroughly rinsed with ethanol and dried prior to experiments. Platinum wire was used as a counter electrode and was previously flame annealed. The reference electrode was an Ag/AgCl electrode in a saturated KCl solution, equipped with a bridge to allow operation in organic solvent. All potentials were calibrated using the ferrocene/ferrocenium ($Fc^{+/0}$) redox couple as an internal standard, which was added in solution at the end of each measurement. In DMF, $E_{1/2}$ (Fc^+/Fc^0) = 0.60V vs Ag/AgCl/sat. KCl. Only the second cycle of all CVs are shown, although no difference in consecutive scans has been observed.

Controlled potential electrolysis (CPE) experiments were carried out in a gas-tight two-compartment electrochemical cell with two ceramic-PVDF composite membranes (16 μm thickness, Xuran) separating the anodic and cathodic compartments. The working electrode was a 1 cm^2 glassy carbon plate, the counter electrode was a platinum mesh and the reference electrode was an Ag/AgCl electrode in a saturated KCl solution, equipped with a bridge to allow operation in organic solvent. Anolyte and catholyte contained DMF and 2 M of H_2O as the proton source and 0.1 M of $TBAPF_6$ as the electrolyte. Only in the catholyte 1 mM of complex **1** was added. Both solution compartments were saturated with CO_2 during at least 20 minutes before starting the electrolysis, but no more gas was bubbled during the electrolysis. The experiments were conducted at room temperature under stirring at the cathode side. The volume of solution held by the cell in total was 22.6 mL, with ca. 10.6 mL of total headspace volume.

Gas products were quantified by gas chromatography (Model 8610C SRI Instruments) equipped with TCD and FID detectors from 50 µL aliquots of the headspace of the cathode compartments. Hydrogen (H_2) and carbon monoxide (CO) were detected by thermal conductivity detector (TCD) and flame ionization detector (FID), respectively. Liquid products were evaluated using an ionic exchange chromatograph (Metrohm 883 Basic IC) equipped with a Metrosep A Supp 5 column and a conductivity detector.

The faradaic yields were calculated by quantifying the products in the head-space gas of the cathodic side, on the basis of Equation 1:

$$Faradaic\ efficiency = \frac{N \times F \times n}{Q} \times 100 \qquad (1)$$

Where Q, F, and N represented the charge passed through the system (C), Faraday's constant (C mol^{-1}), and moles of H_2/CO generated, respectively. In the reaction process, 2 moles of electrons were consumed to produce 1 mole of product, therefore $n = 2$.

Electrodes preparation and characterization

The electrodes used a 3 cm x 1 cm gas diffusion layer (GDL, AVCarb GDS 3250, Fuel Cell Store) strip, which was briefly sonicated in EtOH and let dry in air before utilization. MWCNTs (Sigma) were used after acid treatment as following: the raw MWCNTs material were dispersed in H_2SO_4 (2 M), sonicated for 1 h at ambient temperature, washed repeatedly with H_2O, then EtOH and dried in a vacuum oven at 70°C overnight. This acid treated MWCNTs (2 mg) were sonicated for at least 30 min in EtOH (200 µl) containing a solution of Nafion perfluorinated resin (5 µl of a 5 wt% solution in mixture of lower aliphatic alcohols containing 5% water). The suspension was then drop-casted on the GDL (1 cm^2 deposit) and dried in air at 70°C for at least 30 min. Subsequently, the GDL-MWCNT electrode was immersed in a solution of complex **1** in DMF (10 mM) overnight on an orbital shaker at low speed. Finally, the electrode was dried, washed with water then acetonitrile and dried in air.

SEM images were acquired using a Hitachi S-4800 scanning electron microscope. X-ray photoelectron spectra (XPS) were collected using a Thermo Electron Escalab 250 spectrometer with a monochromated Al Ka radiation (1486.6 eV). The analyzer pass energy was 100 eV for survey spectra and 20 eV for high resolution spectra. The analysed area was 500 mm^2. The photoelectron take-off angle (angle between the surface and the direction in which the photoelectrons are analysed) was 90°. Curve fitting of the spectra was performed with the Thermo Electron software Avantage. The electroactive sites were calculated through the integration of the oxidation wave in the CV scan (Figure S9) according to Equation 2:

$$\Gamma Ni = \frac{q}{nFA} \tag{2}$$

Where ΓNi is the number of electroactive sites (mol cm^{-2}), q is the charge (C) obtained from the integration of the oxidation wave, n the number of electrons in the redox process per Ni center (n = 1), F is the Faraday constant (96485 C mol^{-1}), and A is the geometrical electrode area (1 cm^2).[13]

Heterogeneous Electrochemical Studies

Linear sweep voltammetry (LSV) was performed for each sample before CPE, first under Ar and successively under CO_2. Gas was bubbled in the solution for at least 20 minutes before each experiment. The scan rate was 10 mV s^{-1}. CPE experiments were carried out in a gas-tight H-shape cell in which cathode and reference electrode are separated from the anode by an anion exchange membrane (AMV Selemion, ACG Engineering). The solvent used was acetonitrile containing 1% of H_2O, and the electrolyte was $TBAPF_6$ 0.1 M. The cathode used was a GDL on which MWCNs with the complex **1** were drop-casted as described above, the anode was platinum and the reference electrode was an Ag/AgCl electrode in a saturated KCl solution, equipped with a bridge to allow operation in organic solvent. All potentials were calibrated using the ferrocene/ferrocenium ($Fc^{+/0}$) redox couple as an internal standard, which was added in solution at the end of each measurement. In acetonitrile, $E_{1/2}$ (Fc^+/Fc^0) = 0.54V vs Ag/AgCl/sat. KCl. CO_2 gas was bubbled in the solution for at least 20 minutes before each experiment and no more gas was bubbled during the electrolysis. The experiments were conducted at room temperature and under stirring at the cathode side. The volume of solution held by the cell in total was 22.6 mL, with ca. 10.6 mL of total headspace volume.

The electrolysis products (hydrogen, CO and formate) were quantified in a similar manner as in the homogeneous electrochemical studies part. The faradaic yields were calculated by quantifying the products in the head-space gas of the cathodic side, on the basis of Equation 1 (see above).

The following formulas

$$TON = \frac{moles\ of\ product}{moles\ of\ catalyst} \tag{3}$$

and

$$TOF = \frac{TON}{reaction\ time\ [s]} \tag{4}$$

were used to calculate Turnover Number (TON) and Turnover Frequency (TOF) values, respectively.

Acknowledgements

S.P. and D.G. acknowledge financial support from the European School on Artificial Leaf: Electrodes & Devices (eSCALED). This project has received funding from the European's Union's Horizon 2020 research and innovation programme under the Marie Sklodowska-Curie grant agreement No 765376.

*We thank Geoffrey Gontard (Sorbonne Universités) for solving the structure of cis-**1** (DMF).*

We thank Francoise Pillier (Sorbonne Universités) for the SEM images.

References

[1] A. Liu, M. Gao, X. Ren, F. Menga, Y. Yang, L. Gao, Q. Yang, T. Ma, J. *Mater. Chem. A.* **2020**, *8*, 3541–3562.

[2] B. Kumar, J. P. Brian,V. Atla, S. Kumari, K. A. Bertram, R. T. White, J. M. Spurgeon, *Catal. Today* **2016**, *270*, 19–30.

[3] D. Gao, F. Cai, G. Wang, X. Bao, *Curr. Opin. Green Sustain. Chem.* **2017**, *3*, 39–44.

[4] R. Francke, B. Schille, M. Roemelt, *Chem. Rev.* **2018**, *118*, 4631–4701.

[5] K. Elouarzaki, V. Kannan, V. Jose, H. S. Sabharwal, J. M. Lee, *Adv. Energy Mater.* **2019**, *9*.

[6] N. Elgrishi, M. B. Chambers, X. Wang, M. Fontecave, *Chem. Soc. Rev.* **2017**, *46*, 761–796.

[7] C. Sun, R. Gobetto, C. Nervi, *New J. Chem.* **2016**, *40*, 5656–5661.

[8] L. Sun, V. Reddu, A. C. Fisher, X. Wang, *Energy Environ. Sci.* **2020**, *13*, 374–403.

[9] X. M. Hu, M. H. Rønne, S. U. Pedersen, T. Skrydstrup, K. Daasbjerg, *Angew. Chemie - Int. Ed.* **2017**, *56*, 6468–6472.

[10] Y. Wu, Z. Jiang, X. Lu, Y. Liang, H. Wang, *Nature* **2019**, *575*, 639–642.

[11] X. Zhang, Y. Wang, M. Gu, M. Wang, Z. Zhang, W. Pan, Z. Jiang, H. Zheng, M. Lucero, H. Wang, G. E. Sterbinsky, Q. Ma, Y. Wang, Z. Feng, J. Li, H. Dai, Y. Liang, *Nat. Energy* **2020**.

[12] J. D. Blakemore, A. Gupta, J. J. Warren, B. S. Brunschwig, H. B. Gray, *J. Am. Chem. Soc.* **2013**, *17*, 30.

[13] B. Reuillard, K. H. Ly, T. E. Rosser, M. F. Kuehnel, I. Zebger, E. Reisner, *J. Am. Chem. Soc.* **2017**, *139*, 14425–14435.

[14] P. Kang, S. Zhang, T. J. Meyer, M. Brookhart, *Angew. Chemie - Int. Ed.* **2014**, *53*, 8709–8713.

[15] G. Neri, J. J. Walsh, C. Wilson, A. Reynal, J. Y. C. Lim, L. Xaoe, A. J. P. White, N. J. Long, J. R. Durrant, A. J. Cowan, *Phys. Chem. Chem. Phys.* **2015**, *17*, 1562–1566.

[16] A. Zhanaidarova, C. E. Moore, M. Gembicky, C. P. Kubiak, *Chem. Commun.* **2018**, *54*, 4116–4119.

[17] N. J. Youn, J. S. Kim, K. C. Song, S. H. Kim, S. Ahn, S. K. Chang, *Bull. Korean Chem. Soc.* **2005**, *26*, 849–851.

[18] Y. Zhao, D. Xue, H. Qi, C. Zhang, *RSC Adv.* **2017**, *7*, 22882–22891.

[19] J. D. Froehlich, C. P. Kubiak, *Inorg. Chem.* **2012**, *51*, 3932–3934.

[20] J. D. Froehlich, C. P. Kubiak, *J. Am. Chem. Soc.* **2015**, *137*, 3565–3573.

[21] C. Costentin, M. Robert, J.-M. Savéant, *Chem. Soc. Rev.* **2013**, *42*, 2423–2436.

[22] S.Creager, *Handbook of Electrochemistry*, ed. C. Zoski Elsevier, Amsterdam, **2007**, p.101.

[23] P. D. Tran, A. Le Goff, J. Heidkamp, B. Jousselme, N. Guillet, S. Palacin, H. Dau, M. Fontecave, V. Artero, *Angew. Chemie - Int. Ed.* **2011**, *50*, 1371–1374.

[24] T. Qiu, G. P. A. Yap, J. Rosenthal, *ACS Appl. Energy Mater*. **2019**, *12*, 8560–8569.

[25] M. Beley, J. P. Collin, R. Ruppert, J. P. Sauvage, *J. Am. Chem. Soc.* **1986**, *108*, 7461–7467.

[26] Y. Wu, B. Rudshteyn, A. Zhanaidarova, J. D. Froehlich, W. Ding, C. P. Kubiak, V. S. Batista, *ACS Catal.* **2017**, *7*, 5282–5288.

[27] J. H. Kim, A. R. Hwang, S. K. Chang, *Tetrahedron Lett.* **2004**, *45*, 7557–7561.